RSC Advances

1   **First-principles investigation on the structural, electronic**

2   **properties and diffusion barriers of Mg/Al doped NaCoO$_2$ as**

3   **the cathode material of rechargeable sodium batteries**

4   *Jincang Su [a], Yong Pei [a], Zhenhua Yang [b] Xianyou Wang [a,*]*

5   *([a] Key Laboratory of Environmentally Friendly Chemistry and Applications of Minister of*

6   *Education, School of Chemistry, Xiangtan University, Hunan, Xiangtan 411105, China*

7   *[b] Key Laboratory of Low Dimensional Materials & Application Technology of Ministry of*

8   *Education, Xiangtan University, Hunan, Xiangtan 411105, China)*

9

10   **ABSTRACT**：Mg/Al doped NaCoO$_2$ layered transition-metal oxides as a potential

11   cathode materials for sodium ion batteries have been investigated by the

12   first-principle calculations. The effects of divalent Mg ion or trivalent Al ion doping

13   on the crystal structure, electron transfer, the changes of valence, average

14   intercalation voltage and diffusion barriers of NaCoO$_2$ are studied. The DFT

15   calculations indicate NaCoO$_2$ with Mg or Al ions doping will lead to a higher average

16   intercalation voltage, which is beneficial to obtaining high energy density. Charge

17   disproportionation induced by divalent Mg ion doping results in the appearance of

18   electronic holes in Na(Co$_{0.92}$Mg$_{0.08}$)O$_2$, which may enhance its conductivity

19   significantly. The nudged elastic band calculation results indicate that trivalent Al ion

20   doping affects slightly on the diffusion barriers of NaCoO$_2$, but divalent Mg ion

21   doping can significantly decrease the diffusion barriers and enhance Na ion diffusion

22   rate, which is benefit to the improvement of the rate capability.

23

24   **KEYWORDS**：Sodium ion batteries; First principles calculation; Cathode

---

[*] Corresponding author. Tel: +86 731 58292060; Fax: +86 732 58292061.
E-mail address: wxianyou@yahoo.com (X. Wang).

1

25   material; Doping; Electronic structure

1. Introduction

27   Sodium-ion batteries are the most attractive alternative to lithium-ion batteries

28   for electric vehicle propulsion and renewable electric power storage due to their

29   potential advantages of lower cost and abundance of sodium resources[1-5] . The

30   broad application of sodium-ion batteries will bring out substantial relief and

31   expansion of the existing energy storage market, which is now primarily based on

32   lithium-ion technology. To realize sodium-ion technology, a critical issue is to find

33   out suitable host materials that can accommodate sufficient sodium ions for

34   reversible electrochemical insertion reaction. Similar to the lithium ion cathode

35   materials, layered transition-metal oxides have drawn significant attention as cathode

36   materials in sodium-ion batteries. Although the lithium and sodium ions belong to

37   alkali ions, the chemistry of Na layered cathode materials is expected to be different

38   from their Li analogue. At present, a variety of layered sodium transition-metal

39   oxides Na_xMO_2(M=Co, Ni, Mn, V, Fe, Cr, etc.) cathode materials have been

40   reported[6-10] . Among them, Na_xCoO_2 was early examined as intercalation hosts of

41   Na ions *via* chemical sodiation and desodiation[11]   and it becomes a notable cathode

42   material for sodium-ion batteries at present [12-16] . However, the relatively low

43   average intercalation voltage and poor conductivity limit its wider application.

44   Nevertheless, the heavier atomic mass (Li: 6.9 g.mol^{-1}, Na: 23 g.mol^{-1}) and larger

45   ionic radius (Li$^+$:0.76 Å, Na$^+$:1.02 Å) of Na ion make it difficult to intercalate and

46   extract from the layered $NaCoO_2$ crystal. Therefore, the current work is mainly

47   focused on improving the intercalation voltage, electronic conductivity as well as ion

48   mobility which influences the electrochemical performances of sodium ion batteries.

49   In recent years, metal doping in cathode materials have been reported as one of

50   the most significant method to improve the electrochemical performances of layered

51   transition metal cathode materials[17-20] . In this work, divalence Mg ion or trivalence

52   Al ion doping to $NaCoO_2$ was simulated by first principles calculations to study the

53   effect of doping ions on its electrochemical properties. The changes of crystal and

54   electronic structure, electron transfer, diffusion barrier of Mg or Al ions doped

55    $NaCoO_2$ are studied by the calculations of density of states and electron density

56   differences. Furthermore, the detail structural characteristics, average intercalation

57   voltage (AIV), electronic conductivity and ion mobility of Mg or Al ions doped

58    $NaCoO_2$ were predicted.

59   **2. Computational details**

60   The calculations have been performed using the ab initio total energy and

61   molecular-dynamics program VASP (Vienna ab initio-simulation program) developed

62   at the institute für Materialphysik of the Universität Wien[21, 22] . The interactions

63   between valence electrons and ions are described with the projector augmented wave

64   (PAW) pseudo-potentials[22] . The Hubbard U parameter is generally used to ascertain

65   the bandgap and band structure of transition metal compound. Besides, the

66   benchmark calculations indicate that the GGA/PBE+U method with U=4.91 eV for

67   Co-3d electrons taken from the literature[23] results in high-spin magnetic solution to

68   the $NaCoO_2$ compound, which is in contradictory to previous experimental

69   measurements[24] . Though a linear response approach has been proposed to evaluate

70   the effective parameters in the GGA/PBE+U method which could improve the

71   agreement with experiment[25, 26] , for simplicity, the present computational study

72   does not include the Hubbard U parameter. The convergence tests of the total energy

73   with respect to the k-points sampling and cut-off energy have been carefully

74   examined, which ensure that the total energy is converged to 10^{-5} eV per formula unit.

75   The Monkhorst-Pack[27] scheme with $5 \times 5 \times 2$ k-points mesh is used for the integration

76   in the irreducible Brillouin zone. All the calculations are performed in a 12 formula

77    $NaCoO_2$ supercell. The structure of Mg or Al ions doped $NaCoO_2$ consists of

78    $NaCoO_2$ superlattice with the center Co atom substituted by Mg or Al atom as shown

79   in Figure 1. The stoichiometry of this superlattice cell is $Na(Co_{0.92}M_{0.08})O_2$(M=Mg,

80   Al). Energy cut-off for the plane waves is 520 eV. Before the calculation of the

81   electronic structure, both the lattice parameters and the ionic position are fully

82   relaxed. The final forces on all relaxed atoms are less than 0.01 eV/Å. All

83   calculations are performed in a ferromagnetic (FM) ordering since the FM

84   arrangements give lower energies than antiferromagnetic (AFM) arrangement.

85   The nudged elastic band (NEB) method was employed to study the diffusion

86   barriers of Na^+ migration in $Na(Co_{0.92}M_{0.08})O_2$(M=Mg, Al) and pristine $NaCoO_2$ for

87   comparison. The NEB is an efficient method to search the minimum energy pathway

88   and saddle points between the given initial and final positions. It was performed with

89   linear interpolating 11 images between the initial and final configurations of the

90   diffusion paths. The geometry and energy of the images were then relaxed until the

91   largest norm of the force orthogonal to the path is less than 0.02eV/ Å. Each image

92   searches for its potential lowest energy configuration along the reaction path while

93   maintaining equal distance to nearby images. We investigated the diffusion barrier of

94   Na^+ migration in $Na(Co_{0.92}M_{0.08})O_2$(M=Mg, Al) and pristine $NaCoO_2$ for a divacancy

95   mechanism, as proposed previously by Van der Ven *et al* for a dilute vacancy $LiCoO_2$

96   and $NaCoO_2$ supercell[28] .

97   **3. Results and discussion**

98   3.1 Crystal structures and stability of Mg or Al doped $NaCoO_2$

99   The   detail   lattice   parameters   of   full   relaxed $Na(Co_{0.92}Al_{0.08})O_2$,

100 Na(Co$_{0.92}$Mg$_{0.08}$)O$_2$ and NaCoO$_2$ are shown in Table 1. It can be seen that the change

101 in value of lattice parameter *a* of Mg or Al doped NaCoO$_2$ are 0.17% and -0.19%,

102 respectively, which is caused by the ionic radius differences of Mg^{2+}, Al^{3+} and

103 Co^{3+}(r$_{Mg2+}$=0.72 Å，r$_{Co3+}$=0.55 Å, r$_{Al3+}$=0.54 Å). However, the lattice parameters *c* of

104 Mg and Al doped NaCoO$_2$ both increase about 0.43%. These should be related to the

105 differences between the electronic structures of Co, Mg and Al. There exist empty

106 Mg/Al *p* orbitals well above the filled oxygen *p* states with no d states as in Co atom,

107 which will increase coulomb repulsion between the oxygen atoms and lead to the

108 increase of *c* value.

109 To study the relative stability of Mg/Al doped NaCoO$_2$, we further calculate the

110 cohesive energyies(E$_{coh}$) of Mg/Al doped NaCo$_{0.92}$M$_{0.08}$O$_2$. It is well known that

111 cohesive energy can be used as an important index to estimate the stability of

112 materials, the cohesive energy can be calculated using the following equation:

113
$$E_{coh} = \frac{1}{a+b+c+d}(E_{total} - aE_{atom}^{Na} - bE_{atom}^{Co} - cE_{atom}^{M} - dE_{atom}^{O})$$

114 where E_{total} is the energy of Mg/Al doped NaCo$_{0.92}$M$_{0.08}$O$_2$, E_{atom}^{Na}, E_{atom}^{Co},

115 E_{atom}^{M} and E_{atom}^{O} are the energy of Na, Co, Mg/Al and O atoms in freedom states,

116 respectively. Integers *a, b, c* and *d* are number of atoms of Na, Co, Mg/Al and O

117 atoms. Therefore, a more negative cohesive energy (E$_{coh}$) indicates a more stable

118 doped system phase. The calculated cohesive energies of NaCo$_{0.92}$Mg$_{0.08}$O$_2$ and

119 NaCo$_{0.92}$Al$_{0.08}$O$_2$ are -4.76eV/atom and -4.84eV/atom, respectively, which indicates

120 that Mg/Al doped NaCoO$_2$ are all stable, the stability of Al doped NaCoO$_2$ is a little

121 more than that of Mg doped.

122 3.2 Average intercalation voltage

123 The average intercalation voltage can be estimated through the calculations of

124   Gibbs energy of system via the first-principles calculations[29, 30]. The intercalation

125   voltage $\overline{V}$ is given by Eq.(1):

126    $$\overline{V}(x) = \frac{-\Delta G}{F}$$ (1)

127   where ΔG is the Gibbs free energy change for the intercalation reaction, and F is

128   the Faraday constant. Assuming the changes of volume and entropy associated with

129   the intercalation are negligible, the ΔG can be approximated by the potential

130   energy term $\Delta E^{[26]}$, where ΔE is given by the difference in the total energies

131   between NaMO$_2$ and the sum of oxide MO$_2$ and metallic sodium, in which the lattice

132   parameters and atomic coordinates are fully relaxed.

133    $$\Delta E = E_{total}\left(NaMO_2\right) - E_{total}\left(MO_2\right) - E_{total}(Na)$$ (2)

134   where $E_{total}(Na)$ is the total energy of metallic sodium in a body-centered-cubic(bcc)

135   phase. The calculated average intercalation potential for $NaCo_{0.92}Mg_{0.08}O_2$,

136    $NaCo_{0.92}Al_{0.08}O_2$ and $NaCoO_2$ are given in Table 1. It can be seen from Table 1 that

137   Mg and Al substitution in transition metal oxides will lead to higher Na intercalation

138   voltage, which is desirable for obtaining high energy density.

139   3.3 Electronic structure

140   In order to investigate the relationship between electronic structure and properties

141   of Mg/Al doped NaCoO$_2$ material, the total density of states（TDOS）of NaCoO$_2$,

142    $Na(Co_{0.92}Al_{0.08})O_2$ and $Na(Co_{0.92}Mg_{0.08})O_2$ were calculated as shown in Figure 2. It

143   can be seen that the bandgap between the occupied valence bands and empty

144   conduction bands of NaCoO$_2$ is 1.05eV, which show a typical semiconductor

145   character. This is in agreement with the experimental results[14, 24] . In case of the

146   Al-doped $NaCoO_2$, the TDOS is nearly the same to pure $NaCoO_2$, which indicates

147   that Al doping affects slightly on the electronic structure of $NaCoO_2$. However, the

148   electronic hole appears in the TDOS of Mg-doped $NaCoO_2$ and the Fermi level shifts

149   to the valence band. Based on charge balance mechanism: $2Co^{3+} \rightarrow Mg^{2+} + Co^{4+}$,

150   the electronic holes in the cobalt t_{2g} band of Co^{4+} ions are caused by the divalence

151   Mg doping. The appearance of Co^{4+} electronic hole will provide electron-acceptor

152   energy level, which is benefit to electronic transition. Therefore, the electron

153   conductivity of $NaCoO_2$ can be significantly enhanced through doping a small

154   amount of divalent Mg ions.

155   Since the properties of transition metal oxide depend much on the hybridization

156   state of Co-3d and O-2p, the partial density of state (PDOS) for Co-3d and O-2p are

157   further calculated, as shown in Figure 3. It can be seen that the PDOS bands of Co-3d

158   in Figure 3(a) can be assigned to three main parts: the occupied valence band

159   between -7 to -1.5eV is attributed to bonding e_g^b; the occupied band within -1.2 to 0

160   eV is assigned to nonbonding t_{2g}; and the band in range of 1.05 to 2.15 eV

161   corresponds to the unoccupied antibonding e_g^*. It is known that in octahedral

162   symmetry of transition-metal ion[29] , the d_{z2} and d_{x2-y2} atomic orbits lose electron and

163   make σ overlap with the p_x, p_y and p_z orbits of oxygen along the octahedral directions

164   which correspond to the e_g^b and e_g^* bands. While the unoccupied antibonding band

165   e_g^* mainly consists of the metal d states, and the occupied bonding counterpart e_g^b

166   mainly shows oxygen p character. The orientations of remaining d_{xy}, d_{xz} and d_{yz}

167   orbital are away from the oxygen and hence have no σ overlap with oxygen p orbital.

168   These orbital can form a set of nonbonding t_{2g} bands whose width is mainly

169 determined by the Co-Co interaction. So the state distribution of Co-$3d$ in occupied

170 t_{2g} and e_g^b bands indicates the electron number participating in the $3d$-$2p$ bonding.

171 Larger density of states of Co-e_g^b as well as lower density of states of Co-t_{2g}

172 represents a higher Co valence state. As shown in Figure 3(a), compared to PDOS of

173 $3d$ states of Co atoms in pure $NaCoO_2$, the changes in PDOS of Al doped

174 $Na(Co_{0.92}Al_{0.08})O_2$ are very small. However, the increase in the density of states of

175 e_g^b and the decease in the density of states of t_{2g} in Mg-doped $Na(Co_{0.92}Mg_{0.08})O_2$

176 indicate that d electrons move from nonbonding bands to bonding bands, and more d

177 electrons participate in the $3d$-$2p$ bonding, which corresponds to a higher Co valence

178 state. It is consistent with the above analysis. Meanwhile, it can be seen from the

179 PDOS that the bandgap between e_g^b and t_{2g} becomes small after Mg doping which

180 implies that the Co-$3d$ and O-$2p$ have a stronger rehybridization and result in more

181 stronger covalence of Co-O in Mg-doped $NaCoO_2$.

182 To further understand the electronic structures of Mg/Al doped $NaCoO_2$, the

183 electron density differences of $Na(Co_{0.92}Al_{0.08})O_2$, $Na(Co_{0.92}Mg_{0.08})O_2$ and $NaCoO_2$

184 in the section cut from octahedron $[CoO_6]$ equatorial plane are illustrated in Figure 4.

185 In comparison to $NaCoO_2$, the electron density differences of Mg/Al doped $NaCoO_2$

186 have the following characteristics: firstly, the electron densities of all Co atoms have

187 no significant differences in Al doped $Na(Co_{0.92}Al_{0.08})O_2$, which indicates that the

188 valence state of all the Co ions is the same. However, the electron densities of Co ion

189 adjacent Mg ion in $Na(Co_{0.92}Mg_{0.08})O_2$ are less than that far from Mg ions, which

190 indicates that Co ion adjacent Mg ion lose more electron and have a higher valence

191 state. Secondly, the electron densities of O ions adjacent Mg ion in

192 $Na(Co_{0.92}Mg_{0.08})O_2$ are more than that far from Mg ions, which indicates divalent Mg

193 doping in $Na(Co_{0.92}Mg_{0.08})O_2$ will lead to an increasing number of oxygen

194 participation in electron exchange. So the oxygen ions become more closed-shell

195 characteristic than in $NaCoO_2$. In other words, oxygen ions in $Na(Co_{0.92}Mg_{0.08})O_2$ are

196 closer to the -2 valence state[19] , which will lead to a stronger Coulomb repulsion

197 between the oxygen layers.

198   Thus, it is found that the electronic structure vary small with 8% mole Al

199 doping in $NaCoO_2$. However, the charge disproportionation induced by 8% mole

200 divalent Mg doping in $NaCoO_2$ affects both Co and O simultaneously. The electronic

201 holes and the communization of Co-3d and O-2p electrons caused by Mg doping make

202 its better conductivity and stronger Coulomb repulsion between the oxygen layers.

203 3.4 Na Ion Diffusion behavior

204   Na diffusion behavior in the electrode materials is a key factor of the rate

205 capability and energy efficiency of rechargeable Na batteries. So it is important to

206 investigate the Na^+ diffusion kinetics in the electrode materials. According to the

207 transition state theory [31] , the diffusion constant is mainly determined by the

208 activation barrier, that is, lower activation barrier energy means faster diffusion rate.

209 Calculations on minimum energy path of Na diffusion in $Na(Co_{0.92}Mg_{0.08})O_2$,

210 $Na(Co_{0.92}Al_{0.08})O_2$ and $NaCoO_2$ are performed. The calculation results indicate that

211 Na ion moves from one octahedral site to another by passing through an intermediate

212 O_4 tetrahedral site as shown in Figure 5(a), and the calculated diffusion barriers for

213 $Na(Co_{0.92}Mg_{0.08})O_2$, $Na(Co_{0.92}Al_{0.08})O_2$ and $NaCoO_2$ are shown in Figure 5(b). It can

214 be seen that in pristine $NaCoO_2$ host, the calculated activation energy barrier for Na

215 diffusion is 0.35eV. For Al doped $Na(Co_{0.92}Al_{0.08})O_2$ crystal, the activation barrier is

216 0.36eV, which is slightly higher than in $NaCoO_2$ host. While in Mg doped

217 $Na(Co_{0.92}Mg_{0.08})O_2$ host lattice, the computed Na diffusion barriers falls to 0.30eV.

218 According to the Arrhenius equation, the diffusion constant (D) is proportional to

219　exp($-E_{barrier}/K_B T$), where $E_{barrier}$ and K_B are the diffusion energy barrier and

220　Boltzmann constant, respectively. Therefore, it can be concluded that at room

221　temperature the Na^+ diffusion rate in Mg doped $Na(Co_{0.92}Mg_{0.08})O_2$ host lattice is

222　about 7 times faster than that in pristine $NaCoO_2$, which indicate that Mg doping is

223　beneficial to Na diffusion. This might be ascribed to the closed-shell oxygen ions

224　structure in Mg doped $Na(Co_{0.92}Mg_{0.08})O_2$, which will lead to a stronger Coulomb

225　repulsion between the oxygen layers and thus facilitate Na diffusion.

226　## 4．Conclusion

227　First-principles computational methods have been used to study crystal structure,

228　electron transfer, the change of valence, and average intercalation voltage as well as

229　diffusion barriers for the divalent Mg and trivalent Al ions doped $NaCoO_2$. The

230　calculated results indicate that Mg/Al doping will lead to a higher average

231　intercalation voltage, which is beneficial to obtain high energy density. Investigations

232　on electronic structures show that trivalent Al ions doping affect slightly on the

233　electronic structure of $NaCoO_2$. However, divalent Mg ion doping in

234　$Na(Co_{0.92}Mg_{0.08})O_2$ will lead to charge disproportionation, which affect

235　simultaneously the electronic structure of both Co and O. The electronic holes of Co^{4+}

236　and closed-shell O^{2-} caused by Mg doping make its higher conductivity and faster Na

237　diffusion rate. Therefore, compared to trivalent Al ion doping, a small amount of

238　divalent Mg ion doping in $NaCoO_2$ will be much beneficial to improve the average

239　intercalation potential as well as electronic conductivity and enhance Na diffusion

240　rate which make Mg-doped $NaCoO_2$ more attractive for promising cathode materials.

241

242　## Acknowledgements

250

251

252

253

254

255

256

257

258

259

260

261

262

263

264

265

266

267

268

269

270

References

271

272 [1] Palomares V, Casas-Cabanas M, Castillo-Martínez E, et al. Update on Na-Based Battery Materials.

273 A Growing Research Path[J]. Energy Environ. Sci. 2013(12): 2312-2337.

274 [2] Slater M D, Kim D, Lee E, et al. Sodium-Ion Batteries[J]. Advanced Functional Materials. 2012,

275 123(8): 947-958.

276 [3] Ellis B L, Nazar L F. Sodium and sodium-ion energy storage batteries[J]. Current Opinion in Solid

277 State and Materials Science. 2012, 16(4): 168-177.

278 [4] Palomares V, Serras P, Villaluenga I, et al. Na-ion batteries, recent advances and present

279 challenges to become low cost energy storage systems[J]. Energy Environ. Sci. 2012, 5(3): 5884-5901.

280 [5] Kim S, Seo D, Ma X, et al. Electrode Materials for rechargeable sodium-ion batteries potential

281 alternatives to current lithium-ion batteries[J]. Advanced Energy Materials. 2012, 2(7): 710-721.

282 [6] Ding J, Zhou Y, Sun Q, et al. Cycle Performance Improvement of NaCrO2 Cathode by Carbon

283 Coating for Sodium Ion Batteries[J]. Electrochemistry Communications. 2012, 22: 85-88.

284 [7] Vassilaras P, Ma X, Li X, et al. Electrochemical Properties of Monoclinic NaNiO2[J]. Journal of

285 The Electrochemical Society. 2013, 160(2): A207-A211.

286 [8] Komaba S, Yabuuchi N, Nakayama T, et al. Study on the reversible electrode reaction of

287 Na1-xNi0.5Mn0.5O2 for a rechargeable sodium-ion battery[J]. Inorganic Chemistry. 2012, 51(11):

288 6211-6220.

289 [9] Ma X, Chen H, Ceder G. Electrochemical properties of monoclinic NaMnO2

290 [J]. Journal of the Electrochemical Society. 2011, 158(12): A1307-A1312.

291 [10] D'Arienzo M, Ruffo R, Scotti R, et al. Layered Na0. 71CoO2: a powerful candidate for viable and

292 high performance Na-batteries[J]. Physical Chemistry Chemical Physics. 2012, 14(17): 5945-5952.

293 [11] Delmas C, Braconnier J J, Fouassier C, et al. Electrochemical intercalation of sodium in NaxCoO2

294 bronzes[J]. Solid State Ionics. 1981, 3: 165-169.

295 [12] Braconnier J J, Delmas C, Fouassier C, et al. Comportement electrochimique des phases

296 NaxCoO2[J]. Materials Research Bulletin. 1980, 15(12): 1797-1804.

297 [13] Samin N K, Rusdi R, Kamarudin N, et al. Synthesis and Battery Studies of Sodium Cobalt Oxides,

298 NaCoO2 Cathodes[J]. Advanced Materials Research. 2012, 545: 185-189.

299 [14] Delmas C, Braconnier J J, Fouassier C, et al. Electrochemical intercalation of sodium in NaxCoO2

300 bronzes[J]. Solid State Ionics. 1981, 3: 165-169.

301 [15] Kikkawa S, Miyazaki S, Koizumi M. Electrochemical aspects of the deintercalation of layered

302 AMO2 compounds[J]. Journal of Power Sources. 1985, 14(1): 231-234.

303 [16] Shacklette L W, Jow T R, Townsend L. Rechargeable electrodes from sodium cobalt bronzes[J].

304 Journal of The Electrochemical Society. 1988, 135(11): 2669-2674.

305 [17] Shi S, Ouyang C, Lei M, et al. Effect of Mg-doping on the structural and electronic properties of

306 LiCoO2: A first-principles investigation[J]. Journal of Power Sources. 2007, 171(2): 908-912.

307 [18] Ceder G, Chiang Y M, Sadoway D R, et al. Identification of cathode materials for lithium batteries

308 guided by first-principles calculations[J]. Nature. 1998, 392(6677): 694-696.

309 [19] Xu X G, Li C, Li J X, et al. Electronic Structure of Li (Co, Mg) O2 Studied by Electron

310 Energy-Loss Spectrometry and First-Principles Calculation[J]. The Journal of Physical Chemistry B.

311 2003, 107(42): 11648-11651.

312 [20] Zou M, Yoshio M, Gopukumar S, et al. Performance of LiM0. 05Co0. 95O2 Cathode Materials in

313   Lithium Rechargeable Cells When Cycled up to 4.5 V[J]. Chemistry of materials. 2005, 17(6):

314   1284-1286.

315   [21] Kresse G, Furthmüller J. Efficient iterative schemes for ab initio total-energy calculations using a

316   plane-wave basis set[J]. Physical Review B. 1996, 54(16): 11169.

317   [22] Kresse G, Joubert D. From ultrasoft pseudopotentials to the projector augmented-wave method[J].

318   Physical Review B. 1999, 59(3): 1758.

319   [23] Zhou F, Cococcioni M, Marianetti C A, et al. First-principles prediction of redox potentials in

320   transition-metal compounds with LDA+ U[J]. Physical Review B. 2004, 70(23): 235121.

321   [24] Takahashi Y, Gotoh Y, Akimoto J. Single-crystal growth, crystal and electronic structure of

322   NaCoO2[J]. Journal of Solid State Chemistry. 2003, 172(1): 22-26.

323   [25] Cococcioni M, De Gironcoli S. Linear response approach to the calculation of the effective

324   interaction parameters in the LDA+U method[J]. Physical Review B. 2005, 71: 35105.

325   [26] Guss P, Foster M E, Wong B M, et al. Results for aliovalent doping of CeBr3 with Ca2+[J].

326   Journal of Applied Physics. 2014, 115: 34908.

327   [27] Monkhorst H J, Pack J D. Special points for Brillouin-zone integrations[J]. Physical Review B.

328   1976, 13(12): 5188-5192.

329   [28] Van Der Ven A, Ceder G. Lithium Diffusion in Layered Li x CoO2[J]. Electrochemical and

330   Solid-State Letters. 2000, 3(7): 301-304.

331   [29] Aydinol M K, Kohan A F, Ceder G, et al. Ab initio study of lithium intercalation in metal oxides

332   and metal dichalcogenides[J]. Physical Review B. 1997, 56(3): 1354.

333   [30] Aydinol M K, Kohan A F, Ceder G. Ab initio calculation of the intercalation voltage of lithium

334   transition metal oxide electrodes for rechargeable batteries[J]. Journal of Powder Sources. 1997, 68:

335   664-668.

336   [31] Vineyard G H. Frequency factors and isotope effects in solid state rate processes[J]. Journal of

337   Physics and Chemistry of Solids. 1957, 3(1): 121-127.

338

Caption for tables and figures

Table 1 Lattice parameters and average intercalation voltages(AIV) of pure $NaCoO_2$ and Mg/Al doped $NaCoO_2$

Figure. 1 Schematic illustration of the supercell $Na(Co_{0.92}M_{0.08})O_2$(M=Al or Mg) from $NaCoO_2$ unit cell: (a) $NaCoO_2$ unit cell, (b) $Na(Co_{0.92}M_{0.08})O_2$ supercell

Figure. 2 Total density of states of (a) $NaCoO_2$, (b) $Na(Co_{0.92}Al_{0.08})O_2$, (c) $Na(Co_{0.92}Mg_{0.08})O_2$. The vertical line at zero point indicates the Fermi energy

Figure. 3 Partial density of state for Co-3d(left) and O-2p(right): (a) $NaCoO_2$, (b) $Na(Co_{0.92}Al_{0.08})O_2$, (c) $Na(Co_{0.92}Mg_{0.08})O_2$. The vertical line at zero point indicates the Fermi energy

Figure. 4 The electron density differences of (a) $NaCoO_2$, (b) $Na(Co_{0.92}Al_{0.08})O_2$, and (c) $Na(Co_{0.92}Mg_{0.08})O_2$ in two sections cut from octahedron $[CoO_6]$ equatorial plane

Figure. 5 (a) crystal structure schematic of sodium migration path ; (b) calculated diffusion barriers for $Na(Co_{0.92}Mg_{0.08})O_2$, $Na(Co_{0.92}Al_{0.08})O_2$ and $NaCoO_2$

Table 1

Structure	a(Å)	c(Å)	c/a	AIV(V)
$NaCoO_2$	2.9295	15.3862	2.63	3.866
$Na(Co_{0.92}Al_{0.08})O_2$	2.9239	15.4527	2.64	3.946
$Na(Co_{0.92}Mg_{0.08})O_2$	2.9344	15.4528	2.63	4.018

Figure. 1

(a)   (b)

Na
O
Co
M

Figure. 2

3
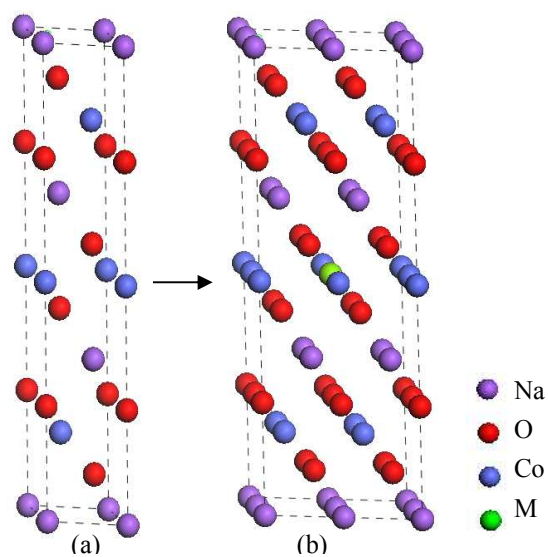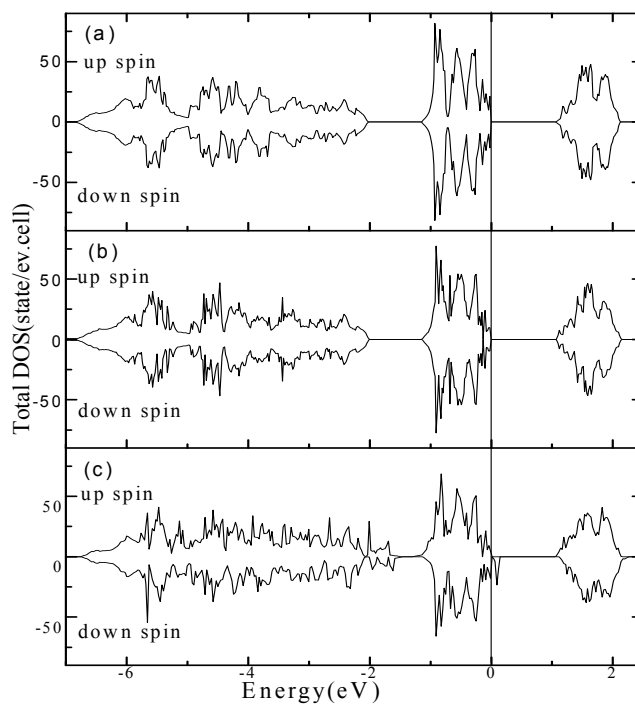
Figure. 3

Figure. 4

Figure. 5

6
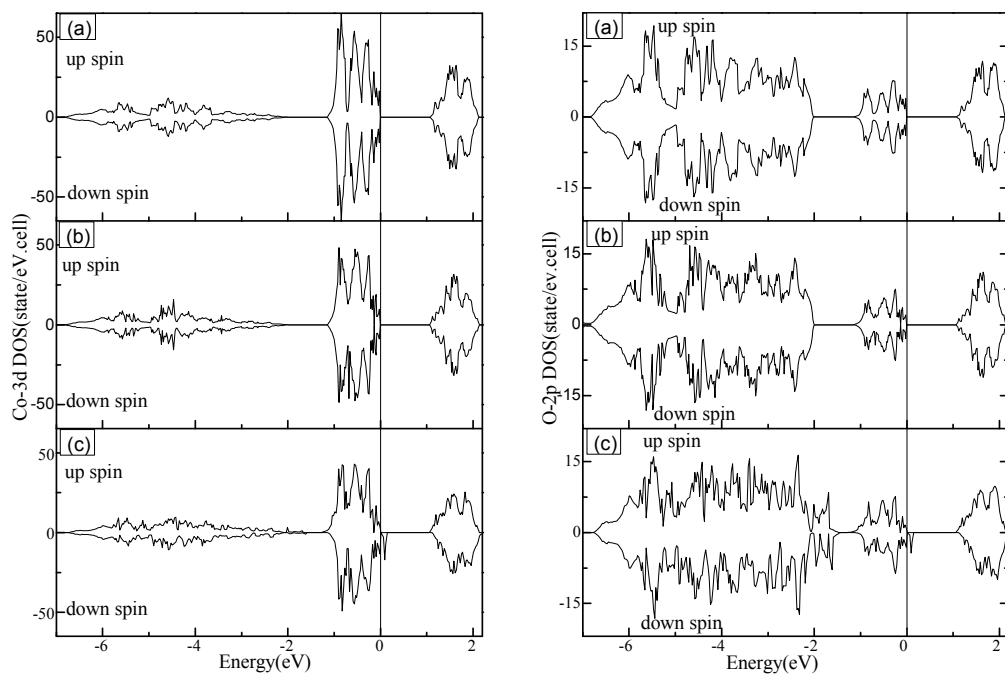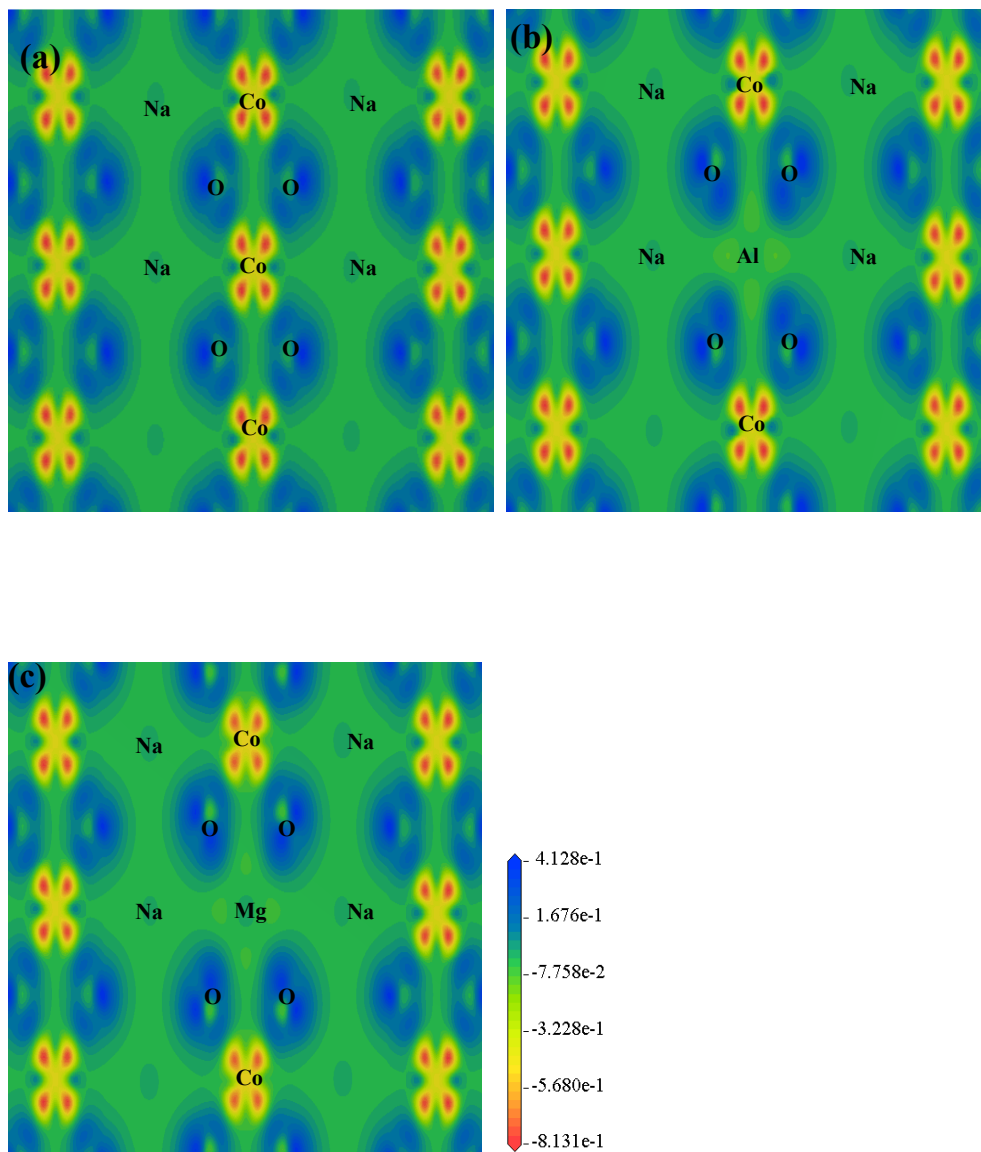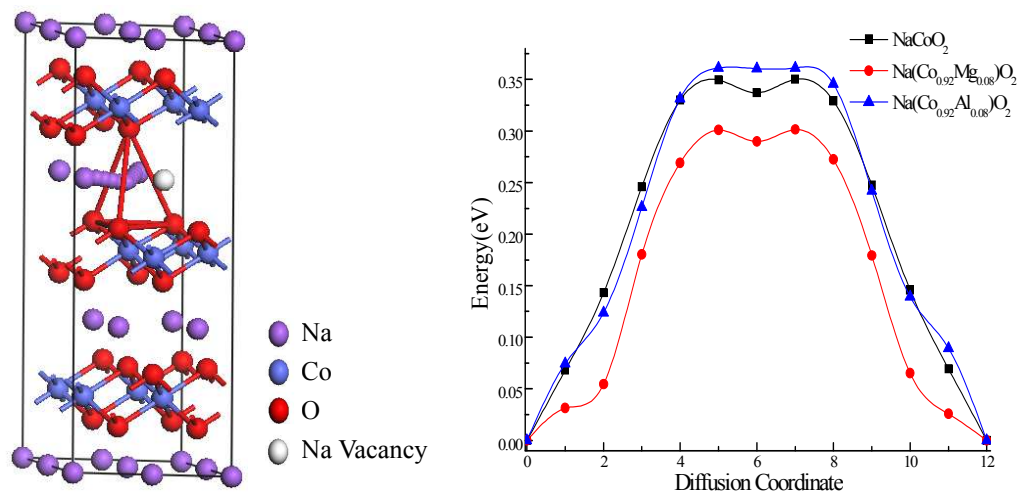
The Table of Contents entry

Graphic:
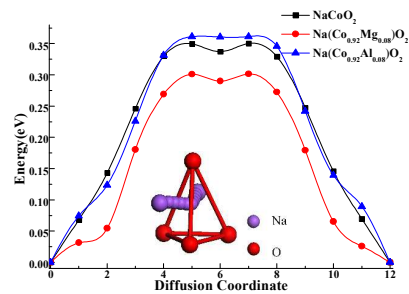
Text: Divalent Mg ion doping in $NaCoO_2$ can significantly decrease the diffusion barriers and enhance Na ion diffusion rate